Directional amorphization of covalently-bonded solids: A generalized deformation mechanism in extreme loading

S. Zhao [1,2], B. Li [3], B.A. Remington [4], C.E. Wehrenberg [4], H.S. Park [4], E.N. Hahn [3], M.A. Meyers [3],*

[1] Beihang University, Beijing, China
[2] University of California, Berkeley, Unite States
[3] University of California, San Diego, Unite States
[4] Lawrence Livermore National Laboratory, United States

Shock compression subjects materials to a unique regime of high quasi-hydrostatic pressure and coupled shear stresses for durations on the order of 1–10 nanoseconds for laser-driven loading of samples. There is, additionally, an attendant temperature increase due to the shock and the mechanisms of plastic deformation in metals whereby dislocations, twins, and phase transitions nucleate and propagate at velocities near the sound speed. Covalently bonded materials have, by virtue of the directionality of their bonds, great difficulty in responding by conventional plastic deformation to this extreme regime of shock compression. We propose that the shear from shock compression induces amorphization, as observed in Si, Ge, B_4C, SiC, and olivine ($(Mg, Fe)_2SO_4$) and that this is a general deformation mechanism in a broad class of covalently bonded materials. The crystalline structure transforms to amorphous along regions of maximum shear stress, forming nanoscale bands, and thereby relaxing the shear component of the imposed shock stress. This process is usually preceded by the emission and propagation of a critical concentration of dislocations.

Keywords: Covalent bonding; Shock compression; Amorphization; Materials under extreme conditions; Peierls Nabarro stress

Introduction

Solid-state amorphization can be created, under prescribed and controlled conditions, by several processes including severe plastic deformation [1], high energy ball milling [2], ion implantation [3], diffusion reaction [4], fatigue [5], and electrochemical means. Levitas [6] authored a broad review on the effect of shear in aiding phase transformations. Shear and compression can reduce the transformation barrier for graphene to diamond [7]. It was demonstrated that the transformation pressure from hexagonal to wurtzitic boron nitride decreases with increasing shear [8]. There is profuse evidence that the presence of shear

assists these structural changes which include amorphization. These approaches were first introduced in metals whose amorphous (disordered) phase has a lower density than their crystalline (ordered) counterpart with a closely-packed lattice. The contribution by Demkowicz and Argon [9] on silicon using the Stillinger–Webber potential reveals that plastic flow is aided by a transformation to a fluid-like phase, which we think is an amorphous structure.

For this reason, solid-state amorphization was typically considered, to a first approximation, as pumping "free-volume" into the crystalline lattice. In this regard, pressure does not aid the process by virtue of the Clapeyron equation, which expresses the change in melting point with pressure as a function of basic thermodynamic parameters. However, this simple picture does

* Corresponding author.
  E-mail address: Meyers, M.A. (mameyers@ucsd.edu)

not account for covalent materials with a structure that is already relatively open because of the directionality of bonds. For example, the unit cells of Si, Ge, and diamond are based on tetrahedra which are accommodated into a cubic structure, leading to a packing factor that is much smaller (0.34) than the face centered cubic (0.74) and body centered cubic (0.68) structures common to metals. Covalent compounds are even more loosely packed, i.e., the packing factors of B_4C (considering the $B_{11}C$ icosahedra as solid spheres) and SiC are approximately 0.14 and 0.35, respectively. Another example is olivine, the major constituent of the Earth's upper mantle, which has a packing factor of 0.4 and shows a partially ionic bonding character. These 'open' structures are prone to collapse upon amorphization. Markenscoff [10] recently developed a theoretical model and attributed the related phenomenon to the pressure-driven "volume collapse instabilities" which give rise to the source of the shear force. Therefore, application of compressive stresses, especially by shock experiments, favors such a process.

Shock compression generates a state of uniaxial strain in materials, propagating at the velocity of the shock wave, which is higher than the longitudinal sonic speed. The resultant stress state can be decomposed in elastic deformation into both hydrostatic ($\sigma_1 = \sigma_2 = \sigma_3$) and shear ($\tau$) stresses (Fig. 1a). The shear stress is shown to generate the localization of deformation, which relaxes the lattice to a hydrostatic state. It was first established by Bridgman [11,12] that shear stresses superimposed on hydrostatic compression decrease the threshold for structural transitions and increase their kinetics. Teller [13] suggested that shear strains could significantly affect the kinetics of reactions. Similar results were obtained by Enikolopyan [14,15]. Thus, there is a growing recognition that shear stresses superimposed on pressure have a significant effect on phase transitions, chemical reactions [16], and solid-state amorphization, the topic of this paper.

The seminal contribution by Jeanloz et al. [17] was the first to show that shock compression can amorphize olivine at a pressure above 56 GPa. This amorphization occurred in regions with high dislocation density and below the pressure at which olivine melts. More recently, Meade and Jeanloz [18] observed amorphization of serpentine ($Mg_3Si_2O_5(OH)_4$) in a diamond anvil cell at pressures between 6 and 25 GPa and suggest that this is a possible source of deep-focus earthquakes at a depth of 100–650 km
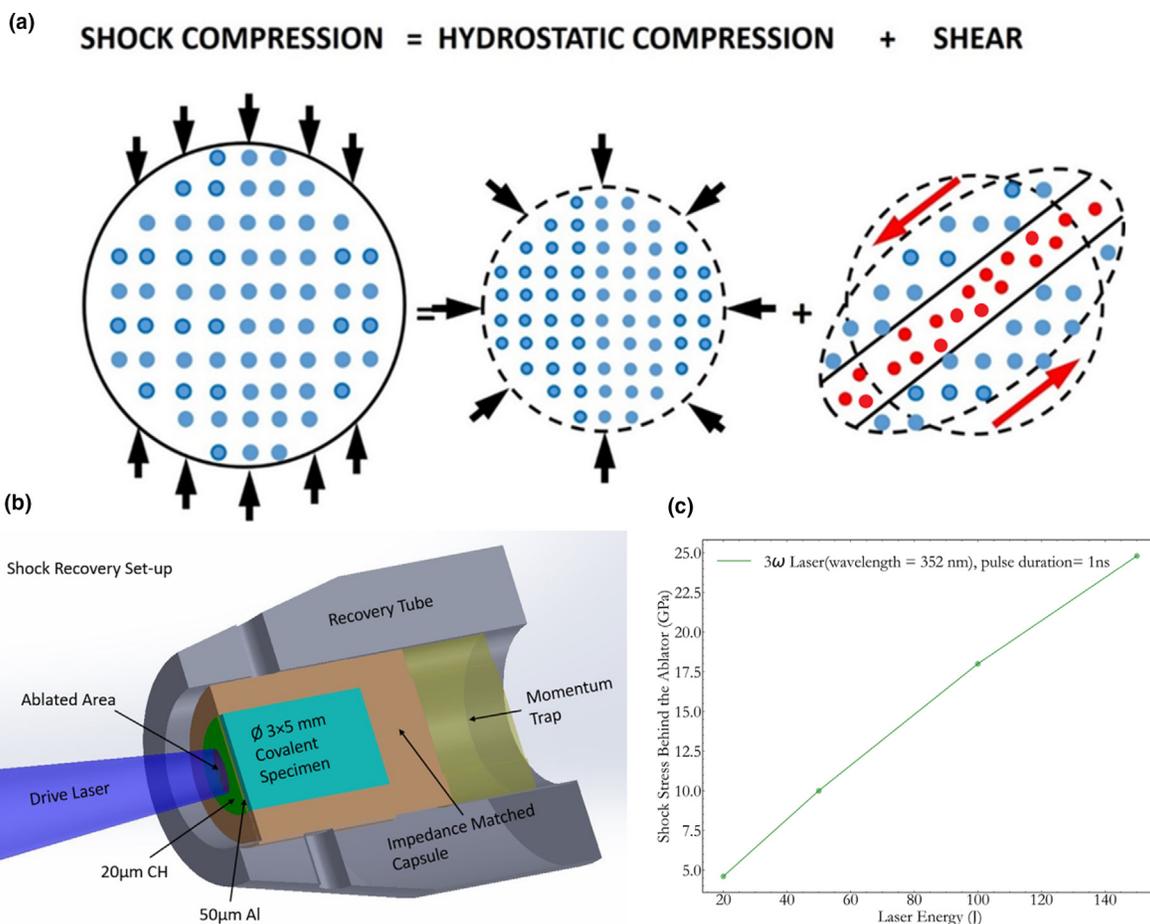
FIGURE 1

(a) Simplified schematic drawing of shock compression and its decomposition into hydrostatic and deviatoric (shear) stresses. The regions of maximum shear stress at 45° actually form a cone. When the surface of the cone is tangential to the slip plane, the resolved shear stress is the maximum and defects will be generated. Here we only highlight one maximum shear, which is 45° away from the principle loading axis. (b) Experimental assembly for laser shock compression of covalently bonded materials; (c) shock stress vs. laser energy.
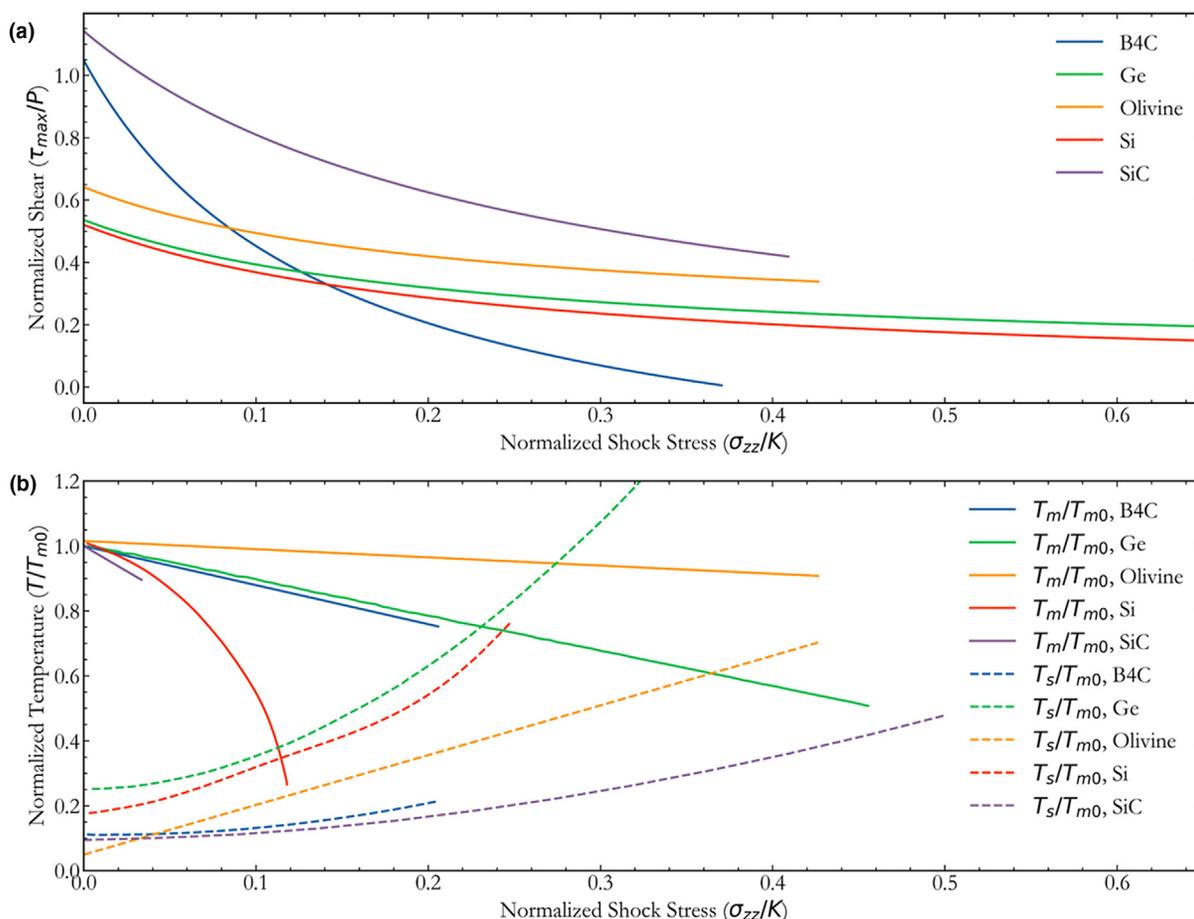
FIGURE 2

(a) The ratio of shear stress, τ, to pressure, P, as a function of shock stress normalized by the bulk modulus, K, for Si, Ge, SiC, B$_4$C, and olivine; (b) Shock temperature/melting point (dotted lines) and melting point for materials with negative Clapeyron slope (solid lines) as a function of shock stress/bulk modulus (data and calculations are in SI).

in the Earth. Smart et al. [19] subjected Si to pressures up to 60 GPa in a diamond anvil cell with simultaneous shear and measured acoustic emissions from the transformation events. The first, and classic paper reporting amorphization in B$_4$C is by Chen et al. [20], who revealed nanoscale amorphous bands in boron carbide recovered from ballistic testing. Reddy et al. [21] observed amorphization in B$_4$C and proposed that dislocations/stacking faults are precursors to it. Their quasistatic experiments using nanoindentation produced a pop-in load that they evaluated to calculate the activation volume. Their Fig. 4 shows the specific mechanism. Although the picture is still not complete, there is compelling evidence that dislocations generated by shear play an important role in amorphization. This behavior triggered intensive experimental [22–24] and computational research [25–27] to refine boron carbide-based armor. This prior work stimulated our exploration into covalent materials as a whole and their propensity to form amorphous bands under extreme loading conditions. Thus, the current results on these deformation mechanisms may provide help to develop a better constitutive understanding not just the materials tested herein but covalently-bonded materials in general.

We used high energy pulsed lasers (Fig. 1b), which can produce pressures up to hundreds of GPa in times on the order of

nanoseconds. This expands the range of extreme conditions beyond the ones possible with gas guns, the traditional means of reaching this regime. The simulated shock stress as a function of laser energy has a triangular shape and the peak shock stress increases with the laser energy (Fig. 1c). The Omega Laser at the Laboratory for Laser Energetics [28] was used for this purpose, in conjunction with specially designed recovery fixtures (Fig. 1b) which enabled post shock recovery and subsequent characterization of the shock-compressed materials. The details on experimental setup are described in the Methods and Materials section. Samples were subjected to shock compression at pressures in the range of 10–100 GPa, then soft recovered for post-shot characterization.

Results and discussion

We subjected five representative covalently bonded solids, two elements (Si and Ge) and three compounds [B$_4$C, SiC, and olivine (Mg, Fe)$_2$SiO$_4$] to shock compression in pursuit of understanding directional amorphization bands.

As shown in Fig. 1a the shear stresses are a direct result of the uniaxial strain state; the lattice is compressed uniaxially in the direction of shock pulse propagation but is not able to expand
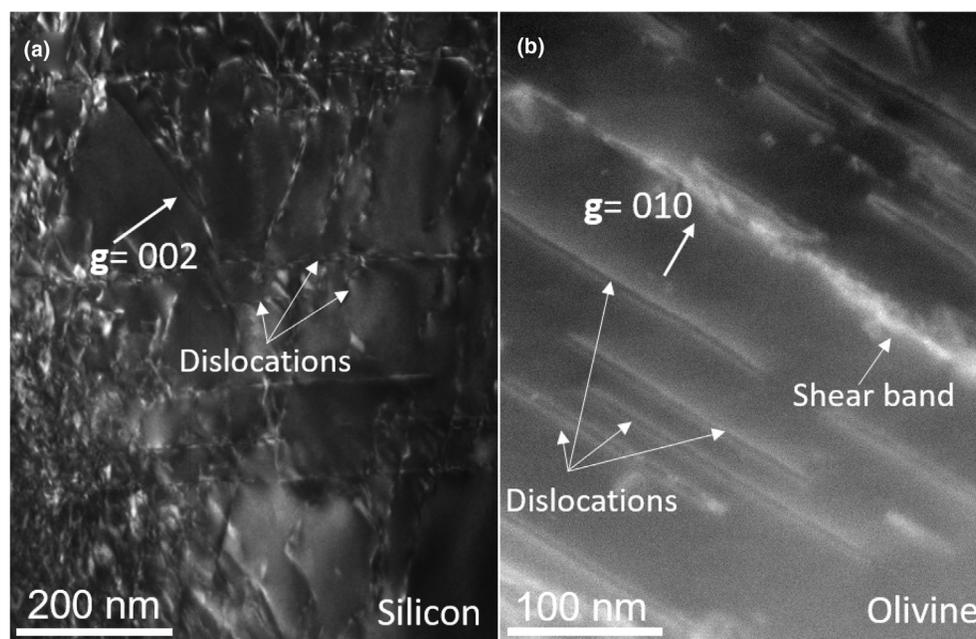
FIGURE 3

Deformation microstructure of the covalently bonded materials below the threshold of amorphization: (a) conventional dark field TEM image of dislocations in silicon; (b) high angle annular dark field image of dislocations in olivine.

laterally because the lateral dimensions of the shocked region ($\sim 10^{-3}$ m) are sufficiently larger than the pulse length ($\sim 10^{-4}$ m). Powerful shear stresses can be generated in conjunction with the uniaxial shock compression, shown in Fig. 2a as a function of a normalized shock stress (divided by the bulk modulus, K). The calculational details are provided in the Supplementary Information section. The ambient shear moduli for the materials studied are: $G_{si} = 79$ GPa [29,30]; $G_{Ge} = 67$ GPa [29,30]; $G_{B4C} = 165–223$ GPa [31,32]; $G_{SiC} = 161–192$ GPa [33,34]; and $G_{olivine} = 78$ GPa [35,36].

Although the ratios of shear stress to pressure decrease with pressure, they are still significant and are the principal contributors to shock-induced plastic deformation. They are relaxed by the generation of defects. The five materials investigated here exhibit a negative Clapeyron behavior; their melting points decrease with increasing pressure (Fig. 2b). This is a direct consequence of the open structures, which collapse upon melting to a higher density. In contrast, in metals the melting point typically increases with pressure, indicative of a positive Clapeyron relation. At a critical shock stress the sample temperature intersects the melting curve. This is the upper limit of our experiments because above this locus we have liquid and not solid-state amorphization. Table 1 provides the melting pressures and experimental shock stresses. Each material was subjected to shock pulses at two or three pressures, except for SiC which was only subjected to one pressure. It decomposes to Si and C at higher pressures. Throughout this paper, we use both the shock stress, σ_{zz}, and the hydrostatic pressure, P. They are related by:

$$\sigma_{zz} = P + \frac{4}{3}\tau_{max} \tag{1}$$

where τ_{max} is the maximum shear stress. In Fig. 2, we use both P and σ_{zz}. σ_{zz} is slightly larger than P.

Metals respond to shock compression primarily through three mechanisms: dislocation generation and motion, twinning, and displacive phase transformations. These structural changes and their formation have been quantified for the past eighty years and are amply documented. In covalently-bonded materials, such as Si or Ge, the dislocation velocity is 4–5 orders of magnitude lower than metallic-bonded material, such as Cu, for the same applied shear stress [37]. The defects generated by shock compression in silicon and olivine investigated here at pressures below the threshold for amorphization are shown in Fig. 3. The specimens were taken from different samples shocked at a much lower peak pressure. These materials exhibit very different crystal structures of low symmetry. It is extremely difficult to tilt the sample to the same imaging conditions. Nevertheless, the morphological difference between dislocations and amorphous bands is reasonably convincing. They consist of parallel arrays of dislocations and stacking faults. However, for SiC no such dislocation arrays were observed and it is proposed that a high density of dislocations is not a prerequisite for amorphization.

Thus, another mechanism is responsible for plastic deformation above a critical stress, namely the formation of amorphous bands, as shown in Fig. 4a–e. These materials were shocked to pressures above the threshold for amorphization (provided in Table 1) and amorphous bands with widths in the nanometer range were generated. There is considerable similarity between the five covalent materials investigated, Si, Ge, B$_4$C, SiC, and olivine. This is the result of the high Peierls-Nabarro stress necessary to move dislocations and of their high self-energy: very high shear stresses can develop in covalent materials, in contrast with metals where these stresses are readily relaxed by dislocation generation and motion.

These amorphous bands are usually preceded, at lower pressures, by dislocations and, in some cases, twins. These defects

RESEARCH: Original Research
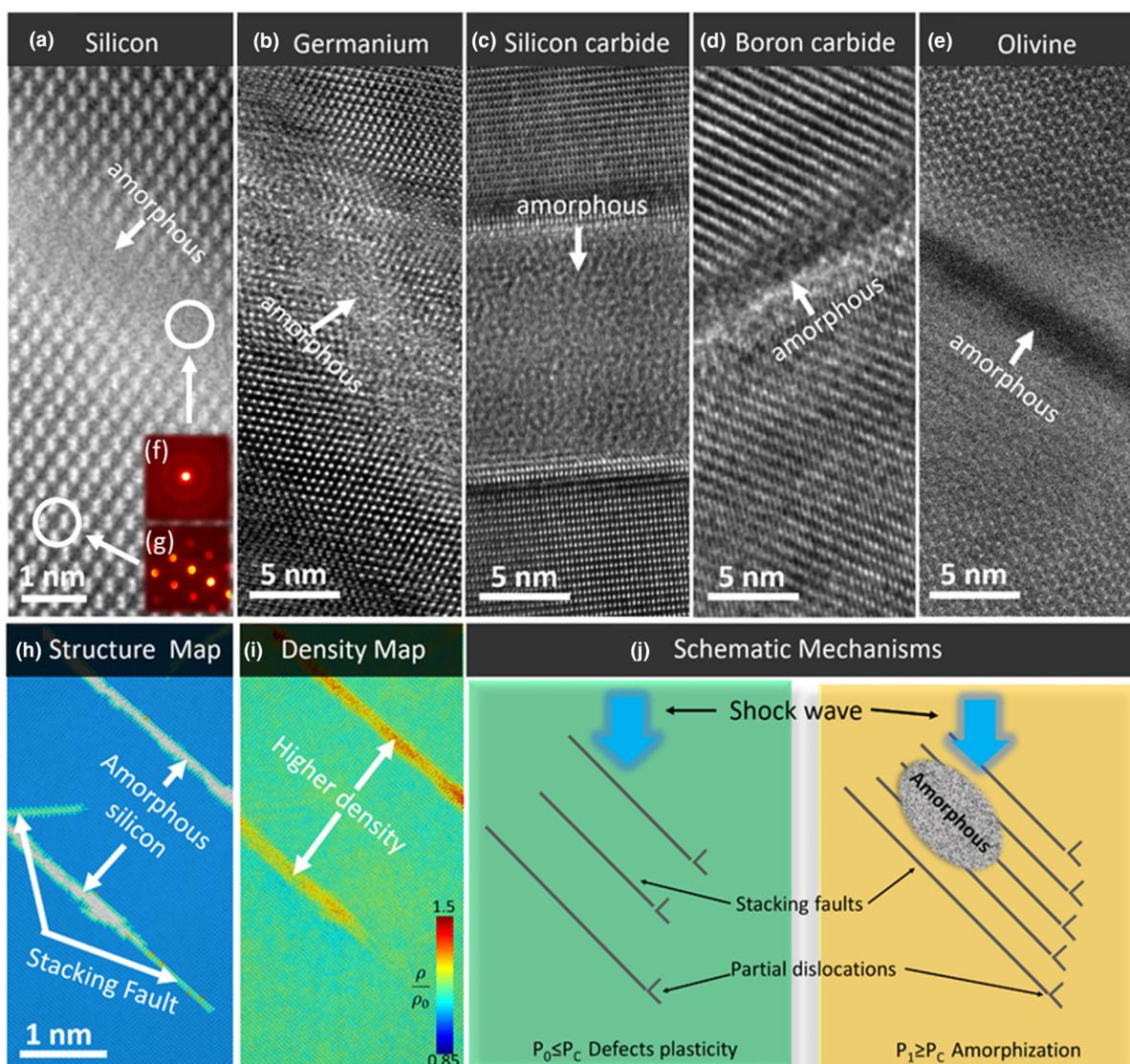
FIGURE 4

Amorphous bands produced by shock compression of (a) Si, (b) Ge, (c) SiC, (d) B$_4$C, (e) Olivine ((Mg, Fe)$_2$SiO$_4$). (f and g) Convergent electron diffraction patterns of amorphous and crystalline silicon, respectively. (h) Molecular dynamics simulation showing stacking faults (light blue) in Si and amorphous region (grey) forming between them. (i) Molecular dynamics simulation of density of the area simulated in 4H. The bands exhibit a higher density by virtue of amorphization. (j) Mechanism for formation of amorphous transformation: Schematic of partial dislocations propagating and leaving behind trailing stacking faults; shock stress is below (left, P$_0$) and above (right, P$_1$) a critical shock stress (P$_c$) for amorphization leading to the formation of amorphous island at P$_1 \geq$ P$_c$.

TABLE.1

Parameters for the five materials investigated.

Material	Melting pressure on the Hugoniot (GPa)	Experimental Shock Stress (GPa)	Shock threshold for amorphization (GPa)	Work of Amorphization, W (10^9 J/m^3)		
				$\sigma_0\varepsilon_t$	$\tau\varepsilon_s$	ρ_dGb^2/2
Si	11.5	4.1; 11; 22.3	11.2	0.548	2.063	0.013
Ge	26	13; 33	13	0.674	2.314	0.310
SiC	122	50	45–50	1.980	13.416	0.478
B$_4$C	100	45–50	25–50	0.489	15.950	0.182
(Mg, Fe)$_2$SiO$_4$	70	54; 56	50–55	0.219	0.918	1.373

form along specific crystallographic planes which have the highest resolved shear stresses. The typical defect structures are shown in Supplementary Information (SI).

The formation of these bands decreases the local shear stresses and relaxes the overall stress state to a near hydrostatic state. The amorphous bands are further confirmed by the diffraction

images of the recovered samples. The diffraction of crystalline structures typically shows the distinct sharp rings or dots which result from the crystalline planes; inside the bands, crystallinity is lost and the pattern shows only a diffused halo, the trademark of amorphization. This is illustrated here for silicon (Inserts to Fig. 4a, f and g), with the other four structures exhibiting similar characteristic amorphous diffraction patterns. Our experiments show that the amorphous structures are retained after unloading. In terms of material properties, this is something under current investigation. The electronic band structure of silicon and germanium is altered by amorphization, which leads to different thermal/optical/mechanical/electrical properties.

The molecular dynamics (MD) simulation for Si shows in a clear fashion how the stacking faults serve, upon reaching a critical concentration level, as the nucleation sites for amorphization (Fig. 4h). Two packets of stacking faults are shown with a nascent amorphous region inside each of them. The stacking faults are shown in light blue and the amorphous region in grey. The simulations were conducted under shock compression produced by an infinite piston impact. The increase in temperature is incorporated into the calculations, which use a Tersoff potential. The shock propagation direction is the same as the experiments: [001]. The 50 µm Al serves as both a heat shield and a medium to transfer the shock generated by the ablation of the very hot CH through to the covalent target. Especially for the short duration of the MD simulation, this means that the temperature at the Al/Si interface matches the ambient conditions, i.e., about 293 K, which is the starting temperature of the silicon simulations. After that, the temperature evolves due to shock induced temperature rise. The identification of the diamond cubic vs disordered structure was completed using OVITO [38] using the built-in "identify diamond" method, which is an adaptation of the more common Common Neighbor Analysis (CNA) method to second nearest neighbors [39]. Greater details on the molecular dynamics simulations are provided in the Supplementary Information. These stacking fault-defects provide the local stress fields that nucleate the amorphous phase. The process of amorphization is accompanied by an increase in density by virtue of the negative Clapeyron relationship and this is more clearly evident in MD-derived density plots (Fig. 4i). Note that the amorphous phase may also be a consequence of a virtual melting process, i.e., melting below the melting point, when a large nonhydrostatic stress is present [40]. Recent MD simulations in Si [41] under dynamic loading, show that dislocations can move at stresses much below the τ_{PN}. However, the accuracy of the estimation of τ_{PN} (or any other parameters related to the force field) using MD simulation is largely limited by the interatomic potential used. τ_{PN} is also temperature dependent. The temperature increase is not induced by laser directly, but by shock deformation. If the deformation temperature is reduced, for example, in a quasi-isentropic loading condition, amorphization should also occur. In fact, even in quasi-static loading conditions, silicon has been shown to undergo amorphization. The critical barrier should also vary as a function of temperature. This is because the mobility of defects is significantly increased by temperature. Under dynamic loading, the temperature rise at the shock front may generate a lower τ_{PN} and thus make dislocation motion easier. However, it is still much higher than for

metallically-bonded materials. High τ_{PN} is a characteristic of many covalently bonded materials. τ_{PN} and Gb^2 (at zero K) can be useful indicators of amorphization under extreme loading conditions, though the detailed mechanism is material dependent.

Fig. 4j shows in a schematic fashion arrays of stacking faults and/or dislocations below and above the threshold for amorphization. As the pressure is raised beyond a critical value P_c, the partial dislocation density increases and so does their interactions through intersection and pile-ups, generating localized stresses that eventually trigger the nucleation of amorphized regions. Amorphous islands are formed within these regions of high defect concentration. Thus, the shock wave advances, generating in its wake stacking faults which, upon interaction, give rise to amorphization. This structural change takes place in bands at orientations close to 45° to the front, corresponding to the orientation of maximum shear stress τ_s. The dislocations have a periodic spacing which relaxes the shear stresses in the lattice (Fig. 3).

There exist theoretical analyses of this class of structural transitions at different degrees of complexity. The Patel-Cohen [42] and Eshelby [43,44] treatments provide an underlying energetics justification for the combined effects of hydrostatic and shear stresses on the thermodynamics. Levitas [45] provides a comprehensive theoretical framework for this effect, incorporating the effects of external, internal, and transformation (Eshelby) stresses and strains on the structural changes. Indeed, the shear strains produced by shear stresses generate greater relative atomic motions than hydrostatic stresses and strains in shock compression. The expression for the work per unit volume, W, for the transformation for a stress state where only normal stresses operate in the unit cube aligned with the shock propagation direction (Fig. 1a) can be written as:

$$W = a_1\sigma_0\varepsilon_t + a_2\mathbf{S}\varepsilon_s + E_d + \gamma A \geqslant \Delta G_a(T) \qquad (2)$$

where ε_t is the spherical compression strain and ε_s the deviatoric component of strain in a stress-free transformation, σ_0 is the hydrostatic stress $((\sigma_{11} + \sigma_{22} + \sigma_{33})/3)$, $\mathbf{S}$ is the deviatoric stress tensor, a_1 and a_2 are material parameters which dictate the evolution of one structure to the other. The term E_d, representing the energy per unit volume of the local defect structure $(=\rho_d Gb^2/2$, where ρ_d is the local density of dislocations prior to amorphization, G is the shear modulus, and b is the Burgers vector), is added to Levitas' equation as well as γ, the interfacial energy (A being the interfacial area). Here, ΔG_a (T) is a critical temperature-dependent value of the energy per unit volume that has to be overcome for the transformation to take place (activation energy). For $a_1 = a_2 = 1$, Eq. (2) reduces to the Patel-Cohen formalism. We apply it here to amorphization. In shock compression, the term ε_t is the strain generated by the change of crystalline and amorphous phase. As a first approximation, the shear strain is taken to be that for twinning, 0.707. We assume that when each slip plane has a partial dislocation, amorphization takes place. This results in that value, which can be calculated from the Burgers vector for partial dislocations. The shear strain for twinning in fcc (and its derivatives) is 0.707 [46], and $\mathbf{S}$ is reduced to the local shear stress, τ (Fig. 2a). Thus, Eq. (2) is reduced to:

$$W = \sigma_0\varepsilon_t + \tau\varepsilon_s + \rho_d Gb^2/2 \geqslant \Delta G_a(T) \qquad (3)$$

The shear stresses, shear strains, and energy of dislocation per unit length are given in Table 2 for the experimental pressures at which the five materials were subjected. The corresponding results of energy calculations are presented in Table 1. For all five materials, the energy due to the relaxation of the shear stresses, $\tau\varepsilon_s$, is the largest. The elimination of shock-induced defects can also play a significant role. This analysis does not consider the interfacial energy, γA, because it is dependent on shape and volume.

Eq. (3) indicates that the likelihood to form amorphous bands during plastic deformation is connected to the dislocation activity. The Peierls-Nabarro stress barrier, τ_{PN}, which has to be overcome for dislocations to move is higher, by orders of magnitude, in covalently bonded materials such as Si, ($\tau_{PN}/G \sim 10^{-1}$), than in metallic face centered cubic materials such as Cu ($\tau_{PN}/G \sim 10^{-5}$–10^{-4}) and body centered cubic ($\tau_{PN}/G \sim 10^{-3}$–10^{-2}) materials such as Ta (here G is the shear modulus). Consequently, the average dislocation velocities for covalently-bonded materials such as Si are 4–5 orders of magnitude lower than for an fcc metal such as

Cu for the same applied shear stress [37]. Fig. 5 provides a graphical representation of the Peierls-Nabarro stresses for a number of materials [47]. The normalized Peierls-Nabarro stress (divided by the shear modulus, G) is plotted against the normalized dislocation energy per unit length, $Gb^2/2$, (where b is the Burgers vector), divided by the thermal energy at the melting temperature, kT_m. There is a clear correlation between these two parameters: as the dislocation energy per unit length, $Gb^2/2$, increases, so does the PN stress, τ_{PN}, until it saturates at the theoretical shear stress ($G/2\pi$). The correlation between the normalized τ_{PN} and a normalized dislocation energy per unit length is not for a single class of material (fcc, bcc, hcp, covalent) but for all materials. If one looks at the plot, one can see that each class occupies a small area indicated by its corresponding ellipse. Representative materials of each class are inserted into the ellipses. However, for the totality of materials, there is a definite trend with the curve saturating at the theoretical strength. While it is true that the high Peierls-Nabarro stress in covalent materials is well known, it is convenient to use this intrinsic property of the materials together with the dislocation line energy as a guiding principle

TABLE.2

Experimental shock pressures for the five materials investigated and corresponding shear stresses, dislocation densities, and dislocation energy per unit length $Gb^2/2$.

Material	P (GPa)	ε_V	τ (GPa)	γ	ρ_d(m^{-2})	$Gb^2/2$ (GPa·nm^2)
Si	7.31	0.075	2.917	0.707	7.826E+15	1.671
Ge	8.64	0.078	3.274	0.707	1.733E+17	1.788
SiC	24.45	0.081	19.166	0.7	2.359E+17	2.026
B$_4$C	34.96	0.014	11.280	1.414	3.248E+15	56.162
Olivine	36.46	0.006	13.907	0.066	1.466E+17	9.364
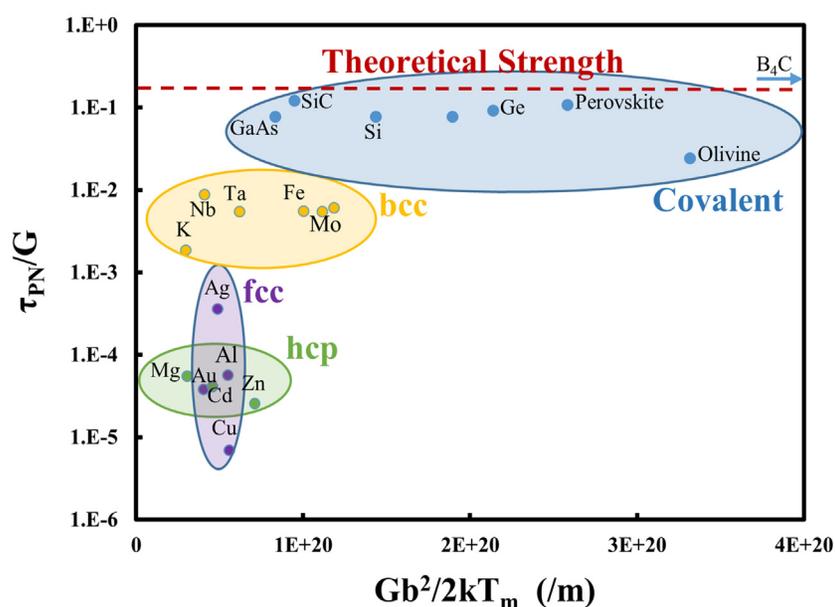
FIGURE 5

Paradigm of materials with different Peierls–Nabarro stresses (τ_{PN}) and dislocation line energies. Covalently bonded materials usually exhibit a higher τ_{PN} stress that is close to the theoretical strength of the material. This renders dislocation activity difficult and triggers brittle fracture under quasi-static conditions. On the other hand, when they are subjected to high stress states in confinement and/or during high strain rate deformation, amorphization emerges as an alternative deformation mechanism to release the applied deviatoric stress. Peierls-Nabarro stress for metals and covalently bonded materials are shown as a function of the ratio between dislocation energy and kT_m, where k is Boltzmann constant and T_m is the melting point (data from Kamimura et al. [47] and other sources (SI)).

to screen the materials which can undergo the amorphization. Both the energy of dislocations and the stress that has to be exerted on them to move (τ_{PN}) are much higher for covalently bonded materials than for metals. The amorphization tendency is enhanced by three factors: (1) a higher PN stress makes plasticity more difficult and thus allows higher deviatoric stresses to build up in the material, which, in turn, promotes directional amorphization; (2) once dislocations are generated, the higher line energy associated with them renders the dislocated area energetically less favorable; and (3) higher stress states lead to higher dislocation velocities (with possible supersonic bursts of dislocations) which eventually determines the kinetics of amorphization. The more open structures and higher interatomic bonds of covalent and ionic materials make them more amenable to amorphization.

Conclusions

We demonstrate that five fully or partially covalent materials (Si, Ge, B_4C, SiC, and olivine $(Mg, Fe)_2SiO_4$) undergo amorphization in shock compression beyond a threshold stress, and propose that an entire class of covalently-bonded materials having an open structure (e. g., diamond, $CaSiO_3$, some perovskite-type compounds, Fe_3B, $AlPO_4$, Nb_2O_5, and ice) will exhibit the same phenomenon under extreme loading. The thermodynamic requirement is that the energy gain upon the collapse of the crystalline structure and its amorphization is sufficient to overcome the activation barrier for the nucleation of the new structure. Shock compression is not a sine qua non condition for amorphization; these amorphized bands have been observed in conventional deformation of an intermetallic ($SmCo_5$) [48], giving additional evidence for the generality of this phenomenon. Shear-induced amorphization of SiC was also observed under quasi-static loading [49]. However, it was reversible, and disappeared under pressure release in a way like "pressure quenching" when the high pressure (stress-state) phase can be frozen in when the stress is released within a very short period of time. Fe_2SiO_4 has been amorphized in static pressure experiments [50]. The role of defects on amorphization is still debated. Morphologically, amorphous shear bands appear to be analogous to a mode II in-plane shear fracture. In a material with well-defined slip systems such as Si and Ge, the amorphous bands follow the slip planes initially. After more generalized amorphization the 45° orientation takes over. In a material without a well-defined slip system, the maximum shear direction seems to be aligned with the amorphous band. They should align themselves predominantly along the maximum shear direction, which is 45° inclined to the loading direction. Previous work on Si [46] included a detailed analysis of the maximum resolved shear stress (at 45° to the shock propagation direction) and the slip planes {111} and directions (35.3° to the shock direction). The orientation of the Si crystal was [001]. The corresponding angle of slip system closest to maximum with the shock direction is 35.3°. So, partial dislocation activity starts on this system. Upon amorphization, the angle rotates to 45° because slip constraints are relaxed. Most of our observations seem to indicate that the dwelling plane of amorphous structures often deviates from the maximum shear cone and follows the slip planes of dislocations or twins, further suggesting that crystalline defects are the precursors to amorphization. We propose this for Si, Ge, B_4C, and olivine. A specific mechanism is proposed for Si [46]. The slip plane is usually close-packed, as it provides the minimum energy penalty for dislocations to successively glide through. Similar to moving a dislocation, the propagation of amorphous bands will tend to follow the most energy-efficient pathway. Therefore, propagation along the Burgers vector on the slip plane seems to be the preferred path. The closeness of the amorphization pathway and the slip system also enables the material to accommodate the arbitrary shape change without undergoing catastrophic failure. It is also entirely possible that the amorphization can occur without dislocations, as was shown in a $SmCo_5$ intermetallic [48] and SiC. SiC actually has many polymorphs, making the situation more complex. It has been shown that shock alters the polymorph distribution in this material and this could be occurring but has not been documented by us. Nevertheless, directional amorphization serves as a new and intriguing deformation mechanism under extreme loading conditions, especially at high stresses, strains, and/or strain rates.

This new deformation mechanism could upend our current understanding of constitutive models. A wide range of brittle materials can be described with similar constitutive models where, when shock loaded above the elastic limit, the strength is constant with pressure [51]. B_4C is seen as an exception to this pattern, and amorphization has been shown to play a determining role in the undesirable softening behavior of armor materials subject to impact loading [20,52]. This work shows that B_4C, with a low work of amorphization and low threshold for amorphization, is likely not an exception to the rule but merely begins amorphization at lower pressure. A wide range of materials may enter new regimes of deformation once loaded beyond the threshold for amorphization, and such a change in our understanding of strength will have a significant impact in a number of fields. This phenomenon can be of importance in planetary sciences by contributing to deep earthquakes through the generation of stress waves upon the compressive collapse of the structure, a phenomenon which may be captured by the acoustic emission [50]. It also has implications in meteor impact because of the shock waves involved.

Methods and materials

Laser shock compression

The Omega Laser at the Laboratory for Laser Energetics [28] was used to shock recovery brittle covalent solids after extreme loading conditions. Si, Ge, SiC and olivine are single crystals and B_4C is polycrystal in our experiments. We could not procure single crystalline B_4C. This is being pursued by researchers at the Army Research Laboratory in search of the fundamental mechanisms of amorphization in this important armor material under ballistic impact. They all have a high purity. Fig. 1b shows the specimen, capsule and recovery tube filled with Aerogel (a glass foam with a density as low as $1000 \ g/m^3$) intended to decelerate and capture the specimen and recovery capsule. The initial duration of the triangular pressure pulse is ~10 ns and the pressure decays monotonically as a function of distance from the laser energy deposition surface. The laser impinges on a polymer (CH), vaporizing it and creating a plasma. The pressure from the plasma launches a shock wave into the material under study.

The free surface velocity is measured by VISAR. This enables, through the software HYADES, the calculation of the pressure as a function of distance from the surface. The use of impedance matched capsules is essential to the successful recovery of the specimens and their subsequent characterization, since covalently bonded materials are brittle. The acoustic impedance (product of sonic velocity and density) close to that of the materials under study is chosen, so that tensile pulses in the material are minimized. The shock stresses are determined by the laser energy as well as by the equation of state of the material. Representative values for Si are plotted in Fig. 1c. We did not grind the post-shock samples to protect the areas subjected to laser shock. TEM specimens were prepared by focused Ga ion beam milling (FIB). Initial coarse milling was done at 30 kV and 5 kV, whereas a final polishing at 2 kV is used to minimize the damage. The defect structure survived in the procedure.

Intellectual Property

We confirm that we have given due consideration to the protection of intellectual property associated with this work and that there are no impediments to publication, including the timing of publication, with respect to intellectual property. In so doing we confirm that we have followed the regulations of our institutions concerning intellectual property.

Research Ethics

We further confirm that any aspect of the work covered in this manuscript that has involved human patients has been conducted with the ethical approval of all relevant bodies and that such approvals are acknowledged within the manuscript. The authors also would like to thank Prof. Xanthippi Markenscoff for valuable discussions and Dr. Zezhou Li for the help with the schematic drawing.

CRediT authorship contribution statement

S. Zhao: Conceptualization, Writing - original draft, Writing - review & editing. **B. Li:** Writing - original draft, Writing - review & editing, Formal analysis. **B.A. Remington:** Supervision. **C.E. Wehrenberg:** Investigation. **H.S. Park:** Conceptualization, Investigation, Methodology. **E.N. Hahn:** Software, Formal analysis. **M.A. Meyers:** Conceptualization, Writing - original draft, Writing - review & editing, Project administration.

Declaration of Competing Interest

The authors declare that they have no known competing financial interests or personal relationships that could have appeared to influence the work reported in this paper.

able discussions and Dr. Zezhou Li for the help with the schematic drawing.

References

[1] M. Peterlechner, T. Waitz, H.P. Karnthaler, Scr. Mater. 60 (2009) 1137–1140.
[2] C.C. Koch et al., Appl. Phys. Lett. 43 (1983) 1017–1019.
[3] A.T. Motta, J. Nucl. Mater. 244 (1997) 227–250.
[4] W. Lur, L.J. Chen, Appl. Phys. Lett. 54 (1989) 1217–1219.
[5] S.H. Mills, Development of Nickel-Titanium-Hafnium Alloys for Impact Resistant Tribology Performances, Colorado School of Mines, Arther Lakes Library, 2019.
[6] V.I. Levitas, Int. J. Plast. (2020).
[7] S. Paul, K. Momeni, V.I. Levitas, Carbon 167 (2020) 140–147.
[8] C. Ji et al., Proc. Natl. Acad. Sci. 109 (2012) 19108–19112.
[9] M.J. Demkowicz, A.S. Argon, Phys. Rev. Lett. 93 (2004).
[10] X. Markenscoff, J. Mech. Phys. Solids (2021) 104379.
[11] P.W. Bridgman, Phys. Rev. 48 (1935) 825–847.
[12] P.W. Bridgman, Proceedings of the American Academy of Arts and, Sciences 71 (1937) 387–460.
[13] E. Teller, J. Chem. Phys. 36 (1962) 901–903.
[14] N.S. Enikolopian, Pure Appl. Chem. 57 (1985) 1707–1711.
[15] N.S. Enikolipyan, Russ. J. Phys. Chem. 63 (1989) 1261-undefined.
[16] N.N. Thadhani, Prog. Mater Sci. 37 (1993) 117–226.
[17] R. Jeanloz et al., Science 197 (1977) 457–459.
[18] C. Meade, R. Jeanloz, Science 252 (1991) 68–72.
[19] T. Smart et al., Appl. Phys. Lett. 115 (2019).
[20] M. Chen, J.W. Mccauley, K.J. Hemker, Science 299 (2003) 1563–1566.
[21] K.M. Reddy, D. Guo, S. Song, C. Cheng, J. Han, X. Wang, Q. An, M. Chen, Sci. Adv. 7 (2021) eabc6714.
[22] K.Y. Xie et al., PNAS 113 (2016) 12012–12016.
[23] G. Parsard, G. Subhash, P. Jannotti, J. Am. Ceram. Soc. 101 (2018) 2606–2615.
[24] A.U. Khan et al., Acta Mater. 157 (2018) 106–113.
[25] Q. An, W. Goddard, T. Cheng, Phys. Rev. Lett. 113 (2014).
[26] Q. An, W.A. Goddard, Phys. Rev. Lett. 115 (2015).
[27] Q. Zeng, A.L. Tonge, K.T. Ramesh, J. Mech. Phys. Solids 130 (2019) 370–392.
[28] Laboratory for Laser Energetics - Wikipedia," can be found under https://en.wikipedia.org/wiki/Laboratory_for_Laser_Energetics.
[29] N. Toupance, Phys. Status Solidi (B) 140 (1987) 361–368.
[30] J.J. Wortman, R.A. Evans, J. Appl. Phys. 36 (1965) 153–156.
[31] Z. Zakhariev, D. Radev, J. Mater. Sci. Lett. 7 (1988) 695–696.
[32] J.D. Clayton, Philos. Mag. 92 (2012) 2860–2893.
[33] R.D. Carnahan, J. Am. Ceram. Soc. 51 (1968) 223–224.
[34] J.D. Clayton, J. Appl. Phys. 107 (2010).
[35] E.H. Abramson et al., J. Geophys. Res. Solid Earth 102 (1997) 12253–12263.
[36] M. Kumazawa, O.L. Anderson, J. Geophys. Res. 74 (1969) 5961–5972.
[37] D. Hull, D.J. Bacon, Introduction to Dislocations, Elsevier, 2011.
[38] A. Stukowski, Modell. Simul. Mater. Sci. Eng. 18 (2010).
[39] E. Maras et al., Comput. Phys. Commun. 205 (2016) 13–21.
[40] V.I. Levitas, R. Ravelo, Proceedings of the National Academy of Sciences, 109 (2012) 13204-13207.
[41] H. Chen et al., Acta Mater. 206 (2021).
[42] J.R. Patel, M. Cohen, Acta Metall. 1 (1953) 531–538.
[43] J.D. Eshelby, Solid State Phys. 3 (1956) 79–144.
[44] J.D. Eshelby, Proc. R. Soc. Lond. A 241 (1957) 376–396.
[45] V.I. Levitas, H. Chen, L. Xiong, Phys. Rev. B 96 (2017).
[46] S. Zhao et al., Acta Mater. 103 (2016) 519–533.
[47] Y. Kamimura, K. Edagawa, S. Takeuchi, Acta Mater. 61 (2013) 294–309.
[48] H. Luo et al., Nat.Commun. 10 (2019) 1–8.
[49] V.I. Levitas et al., Phys. Rev. B – Condens. Matter Mater. Phys. 85 (2012).
[50] Q. Williams et al., J. Geophys. Res. 95 (1990) 21549–21563.
[51] S. Bavdekar, G. Subhash, Int. J. Impact Eng. 118 (2018) 60–66.
[52] A. Awasthi, G. Subhash, Progr. Mater. Sci. 112 (2020) 100664.